Atmospheric Environment 154 (2017) 1–8

Contents lists available at ScienceDirect

Atmospheric Environment

journal homepage: www.elsevier.com/locate/atmosenv

Variation of the vertical distribution of Nabro volcano aerosol layers in the stratosphere observed by LIDAR

Young Min Noh [a], Dong Ho Shin [b, *], Detlef Müller [c]

[a] International Environmental Research Center, Gwangju Institute of Science and Technology (GIST), Republic of Korea
[b] National Institute of Environmental Research, Kyungseo-dong, Seo-gu, Incheon 404-708, South Korea
[c] University of Hertfordshire, College Lane, Hatfield AL10 9AB, United Kingdom

HIGHLIGHTS

- The volcanic aerosol layer in the stratosphere was observed using lidar.
- The aerosol layer show different vertical profiles and optical properties with time.
- Non-spherical particle is more favorable to gravitational sedimentation.
- An e-folding decay time of the layer is 117 days.

ARTICLE INFO

Article history:
Received 28 October 2016
Received in revised form
2 January 2017
Accepted 16 January 2017
Available online 17 January 2017

Keywords:
Lidar
Volcanic aerosol
Nabro volcano
Depolarization ratio
Stratospheric aerosol

ABSTRACT

We present results of the vertical distribution variation of volcanic aerosol layers in the upper troposphere and lower stratosphere. The data were taken with our multiwavelength aerosol Raman lidar at Gwangju (35.10° N, 126.53° E), Korea. The volcanic ash particles and gases were released around 12 June 2011 during the eruption of the Nabro volcano (13.37° N, 41.7° E) in Eritrea, east Africa. Forward trajectory computations show that the volcanic aerosols were advected from North Africa to East Asia. The first measurement of the aerosol layer over Korea was on 19 June 2011. The aerosol layers appeared between 15 km and 17 km height asl (above sea level). The maximum value of the aerosol layer of the particle backscatter coefficient (1.5 ± 0.3 Mm^{-1} sr^{-1}) and the linear particle depolarization ratio at 532 nm (2.2%) were observed at 16.4 km height asl. We continuously probed the upper troposphere and lower stratosphere for this volcanic aerosol layer during the following 6 months, until December 2011. The volcanic aerosol layer showed a single-peak of the particle backscatter coefficient and a comparably narrow vertical thickness at our observation site at the beginning of our observation period (i.e. comparably soon after the initial eruption period). After that initial period the vertical distribution of the plume changed. Multiple peaks and a comparably broad geometrical thickness developed with progressing observation time. The vertical thickness of the volcanic aerosol layer expanded up to 10 km by 3 August 2011. The linear particle depolarization ratios were larger in the lower part of the aerosol layer than the upper part of the aerosol layer. We observed a strong variation of the AOD (aerosol optical depth) in the first two months of our lidar observations. After these two months the AOD gradually decreased with time from September to December 20111 and the maximum particle backscatter coefficients consistently decreased. The corresponding e-folding decay time of the layer AOD was 117 days.

1. Introduction

Particles and trace gases which are injected into the stratosphere by volcanic eruptions are the biggest source of natural pollution in the stratosphere (Robock, 2000). One of the main components of gases from these eruptions are large amounts of sulfur dioxide (SO_2) which increase the optical thickness in stratospheric heights. These layers exert a cooling effect of Earth's atmosphere (Hofmann and Solomon, 1989) and influence chemical processes in the lower stratosphere (Rodriguez et al., 1991; Solomon et al., 1993). The injected SO2 condenses and oxidizes to sulfuric acid particles through homogeneous nucleation (Wu et al., 1994). Stratospheric aerosols have a notable impact on global

* Corresponding author. National Institute of Environmental Research, Kyungseo-dong, Seo-gu, Incheon 404-708, South Korea.
E-mail address: topgunsdh@gmail.com (D.H. Shin).

http://dx.doi.org/10.1016/j.atmosenv.2017.01.033

climate because of their long residence time in the stratosphere and their large-scale dispersion (Hofmann et al., 2009). For example, the volcanic eruption of Mt. Pinatubo (15.14° N, 120.35° E) in the Philippines in 1991 injected approximately 20 Tg SO_2 into the stratosphere (Bluth et al., 1992; Guo et al., 2004) which led to a global-mean cooling effect of the troposphere by approximately 0.5–0.8 K in 1992 (McCormick et al., 1995; Parker et al., 1996). Barnes and Hofmann (2001) reported that the backscatter coefficient (532 nm), when integrated from 15.8 km to 33 km height the Pinatubo aerosols in the stratosphere had returned to near background levels at Mauna Loa (19.53° N, 155.57° W) by mid-1996.

During the past 20 years, ground-based lidars have been demonstrated to be powerful methods for studying geometrical, optical, and microphysical characteristics of stratospheric aerosols (Wandinger et al., 1995; Ansmann et al., 2010; Mattis et al., 2010; Sawamura et al., 2012). Despite these investigations, measurements of stratospheric aerosol properties under ambient conditions are still, and measurements are particularly sparse over Asian sites along the West Pacific Rim, or Ring of Fire (Uchino et al., 2012).

In this paper, we report on 6 months of measurements of a stratospheric aerosol layer that originated from the Nabro eruption (13.37° N, 41.70° E) that occurred in Eritrea, East Africa, on 12 June 2011. The observations were made over Gwangju (35.10° N, 126.53° E), Korea. We present data on the temporal evolution of the geometrical depth of the volcanic aerosol layer, aerosol backscatter coefficients at 532 and 1064 nm, the linear volume and particle depolarization ratio at 532 nm, and the aerosol optical depth (AOD) at 532 nm.

A brief explanation of the lidar system, the retrieval methods, and the trajectory modelling are presented in section 2. The results of the trajectory modelling and the lidar data are shown in section 3. The main findings of this study are summarized in section 4.

2. Methodology

2.1. Lidar system MRS.LEA

We have been developing a novel multiwavelength aerosol depolarization/Raman-quartz/water-vapor/spectrometer lidar system, called MRS.LEA (Multiwavelength Raman/Spectrometer Lidar in East Asia) since 2008. The instrument is used for the characterization of optical and microphysical properties of East Asian aerosols (Müller et al., 2010; Noh et al., 2008, 2011; Noh, 2014; Shin et al., 2010, 2015; Tatarov et al., 2011). The lidar station is located at the Gwangju Institute for Science and Technology (GIST), Republic of Korea (35.10° N, 126.53° E).

The light source of the lidar is a pulsed Nd:YAG laser (Surelite III-10, Continuum) which operates at the wavelength of 1064 nm. The pulse repetition rate is 10 Hz. A frequency-doubling crystal allows for generating linear-polarized laser light at 532 nm wavelength. In order to reduce the divergence of the emitted radiation, we use a beam expander at 532 and 1064 nm. The return signals are collected with a 14-inch Schmidt-Cassegrain telescope (C14, Celestron).

Hamamatsu R7400-20 photomultiplier tubes (PMT) are used to measure signals in the analogue and photon-counting mode at the two 532-nm channels. We detect the parallel-polarized and cross–polarized backscatter signals, respectively. The bandwidth of the interference filters is 1 nm at 532 nm (full width at half maximum = FWHM). A Hamamatsu R3236 PMT with a cooler is used for analogue and photon-counting at 1064 nm. Transient recorders with 12-bit analog to digital converters and 250-MHz photon counters (TR 20-160, Licel) are used for processing the output signals of the PMTs. In high altitudes such as stratospheric heights, the signal-to-noise ratio of the Raman channels and the ultraviolet wavelength channel (signals from elastic backscattering) are comparably low. Therefore we can only use the channels of elastic backscatter signals at 532 and 1064 nm and the depolarization channel at 532 nm for our observations.

2.2. Aerosol optical properties

We present data taken in the upper troposphere (UT) which extends to approximately 10 km height asl (above sea level) and the lower stratosphere (LS) which extends to approximately 24 km height asl. The optical data that describe the volcanic aerosol layers between the UT and the LS were taken with our lidar system under cloud-free conditions during night-time. We had to apply at least 1-hr signal averaging times due to the low power of the emitted laser pulses. We performed signal-smoothing lengths of 400 m for the particle backscatter coefficients and the linear particle depolarization ratio. The Klett-Fernald method (Fernald, 1984; Klett, 1985) was used to determine the particle backscatter coefficients. The calibration point of the backscatter profiles of the raw signals was set between approximately 28 km and 30 km height asl where no particles but only molecules contributed to the measured signals.

We report the total aerosol burden of the volcanic aerosol layer in terms of the AOD at 532 nm wavelength for the height region from 10 km to 24 km height asl. The value of AOD significantly depends on the lidar ratio which is defined as the ratio of the particle extinction coefficient to the particle backscatter coefficient. Mattis et al. (2010) measured lidar ratio of 30–45 sr at 532 nm in the stratosphere. The data were taken between 2008 and 2009 over central Europe with a multiwavelength Raman lidar and describe stratospheric aerosols that originated from numerous eruptions of volcanoes in the Aleutian Islands, Kamchatka, Alaska, and the Kuril Islands. The aerosol layers typically occurred between 5 km and 25 km height asl. Based on the study by Mattis et al. (2010) we chose an average lidar ratio of 38 sr at 532 nm. Sawamura et al. (2012) also used the same value for the analysis of their lidar measurements of the Nabro volcanic aerosol layer.

We used radiosonde data to calculate the atmospheric molecular density from pressure, wind speed and temperature profiles. Radiosondes were launched four times a day (00:00, 6:00, 18:00 and 24:00 UTC) at the Gwangju International Airport which is about 10 km away from our lidar site.

The linear particle depolarization ratio can be used to characterize the shape of the particles. We calculated the linear particle depolarization ratio (δ^p) at 532 nm according to the following equation (Biele et al., 2000; Freudenthaler et al., 2009):

$$\delta^{\mathrm{p}} = \frac{\beta^{\mathrm{m}}\left(\delta^{\mathrm{v}} - \delta^{\mathrm{m}}\right) + \beta^{\mathrm{p}}\delta^{\mathrm{v}}\left(1 + \delta^{\mathrm{m}}\right)}{\beta^{\mathrm{m}}\left(\delta^{\mathrm{m}} - \delta^{\mathrm{v}}\right) + \beta^{\mathrm{p}}\left(1 + \delta^{\mathrm{m}}\right)} \quad (1)$$

The linear volume depolarization ratio (particles plus molecules) is denoted by δ^v. The molecular and particle backscatter coefficients are denoted by β^m and β^p, respectively. The molecular (Rayleigh) depolarization ratio is denoted by δ^m. The molecular backscatter coefficient can be calculated from the radiosonde data.

The depolarization ratio of backscatter signals from molecules (pure molecular backscattering) only is needed as input parameter for deriving the linear particle depolarization ratio. This value depends on the actual bandwidth of the interference filters of the lidar receiver as the bandwidth decides on whether the rotational Raman bands are included in the detected signals or not (Behrendt and Nakamura, 2002). We calculated a constant molecular depolarization ratio of 0.44% which takes into account the actual bandwidth of the interference filter (more than 1 nm at the co-polarized and cross-polarized 532 nm) according to Behrendt and Nakamura (2002).

When measuring the linear volume depolarization ratio we need to consider the polarization-dependent receiver transmission factor. Backscatter signals are detected with different efficiencies because the transmission efficiency of the optical elements in the detector channels depends on the state of polarization of the incident light. This dependence can lead to an under- or over-estimation of the detected total signal (Mattis et al., 2009; Tesche et al., 2011). Shin et al. (2015) conducted measurements of the transmission-ratio of the 532S (cross-polarized) and the 532P (co-polarized) channels of our lidar system for the data observed in 2011. Shin et al. (2015) confirm that the accuracy of the linear particle depolarization ratio increases by applying the calculated transmission ratio according to the method suggested by Mattis et al. (2009). Accordingly, we applied the transmission ratio to calculate the linear volume depolarization ratio in this study.

2.3. Air parcel trajectories computed with HYSPLIT and PRCF

The HYSPLIT (HYbrid Single-Particle Lagrangian Trajectory; version 4.9) forward trajectory modeling system (Draxler and Hess, 1997, 1998; Stein et al., 2015) was used to understand the spatial distribution of the transport pathway of the ash aerosol plume and to identify the potential receptor regions after the Nabro volcano erupted on 12 and 13 June 2011.

GDAS (Global Data Assimilation System) atmospheric fields were used in HYSPLIT to produce forward trajectories of air parcels that originated from the Mt. Nabro eruption. The forward trajectories provided us with Lagrangian paths of air parcels in time steps of 1-hr from 12 June to 13 June 2011. This information was used to identify the potential receptor region and the transport pathway of the volcanic aerosol layer. Three-dimensional, 240-hr forward trajectories departing from Mt. Nabro were calculated for every hour. The GDAS model uses a grid-cell size of 0.5° × 0.5° and two different height maps which reach from 0.5 km to 10 km height asl, and from 10 km to 19 km height asl. The trajectories were computed in time steps of 1 h from 12 June (start time in 0000 UTC) to 13 June 2011 (end time in 2400 UTC).

The HYSPLIT forward trajectory modeling data were used to identify the potential receptor contribution function (PRCF). Results of the PRCF provide us with probable source regions that are related to high particle concentrations observed at the receptor area. The PRCF values for the grid cells used in the study domain were calculated by counting not only the trajectories that ended at the cell but also the ones that crossed the cell. The PRCF value for the ij^{th} cell is defined as a conditional probability, and n_{ij} is the number of segment trajectory endpoints n that fall into the ij^{th} cell. In order to reduce the uncertainty in a grid cell that has a small number of endpoints, an arbitrary weight function w was applied when the number of the end points in a particular cell was three times less than the number of average end points for all cells (Polissar et al., 2001). The values of w were assigned as follows:

$$w = \begin{cases} 1.00, & 12 < n_{ij} \\ 0.7, & 6 < n_{ij} < 12 \\ 0.42, & 2 < n_{ij} < 6 \\ 0.17, & n_{ij} < 2 \end{cases} \quad (2)$$

The PRCF values for each cell were plotted on the map, which allowed us to identify the potential receptor regions affected by the Nabro volcano eruption. The map was separated according to the altitude range between 10 km and 19 km height asl and between 0.5 km and 10 km height asl.

3. Results and discussion

3.1. Overview of the Mt. Nabro volcanic aerosol plume

Mt. Nabro has an elevation of 2218 m asl. The volcano is located at the border between Eritrea and Ethiopia in Northeast Africa near the Red Sea. The IASI (Infrared Atmospheric Sounding Interferometer) and the SGVP (Smithsonian's Global Volcanism Program, 2011) detected the first activity of the Nabro eruption at 00:00 UTC on 12 June 2011. Visible plumes were rising to an altitude of 13 km asl and continued emissions were observed for several weeks. The volcanic aerosol plume was detected by the Moderate Resolution Imaging Spectrometer (MODIS) on the Aqua satellite at 10:45 UTC on 13 June 2011 (http://earthobservatory.nasa.gov). An estimated 1.3–2.0 Tg (total mass) of SO_2, ash, and water vapour were injected up to the stratosphere (Clarisse et al., 2012; Sawamura et al., 2012).

The distribution of the PRCF in the study area is shown in Fig. 1. The PRCF map for emissions in the altitude range between 10 km and 19 km height shows that grid cells with high PRCF values appeared mainly in East Asia. In contrast, the PRCF map for emissions from lower altitudes, i.e., in the altitude range between 0.5 km and 10 km height shows grid cells with high PRCF values over Africa and India. This result shows that the potential receptor areas are highly dependent on the vertical injection height of the volcanic material.

3.2. Vertical distribution of the aerosol layers in the UT and LS

We performed nighttime measurements during 6 months from 19 June to 14 November 2011 to study the optical properties and

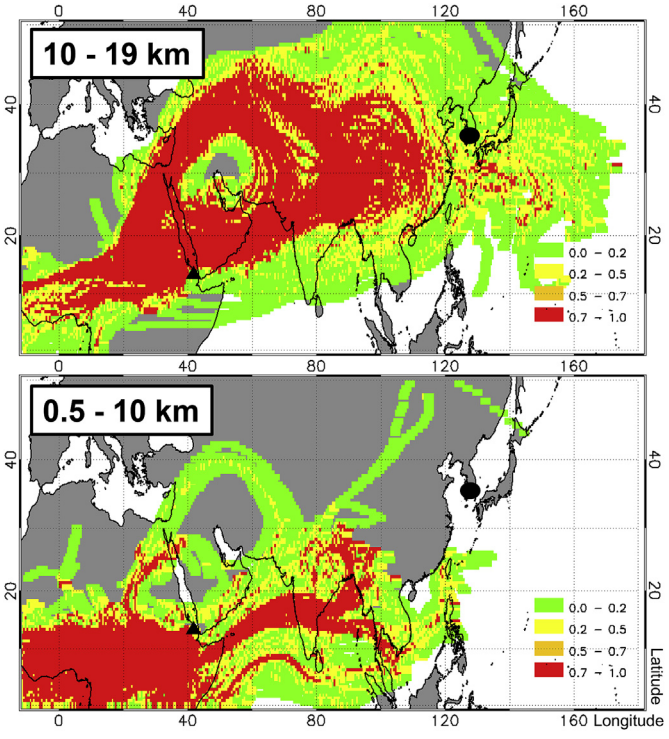

Fig. 1. Potential receptor contribution function (PRCF) maps for transport identification of the plume from the Nabro volcano (black solid triangle). The air parcels were released in the altitude range between 10 km and 19 km height asl (top) and between 0.5 km and 10 km height asl (bottom) in time steps of 1 h from 12 June to 13 June 2011. Colors indicate high potential receptor areas. (For interpretation of the references to colour in this figure legend, the reader is referred to the web version of this article.)

dispersion of the volcanic aerosol layers.

3.2.1. Case study of 19 June 2011: the first measurement of the volcanic aerosol layers

The volcanic aerosol layers in the UT and LS were detected at our observation site for the first time on 19 June 2011, approximately 7 days after the eruption. The aerosol layer peak was observed over Tsukuba, Japan, on 20 June 2011, i.e. about 8 days after the eruption (Uchino et al., 2012). CALIPSO observations showed the stratospheric aerosol layers in South-East Asia approximately during the first 10 days after the eruption (Fairlie et al., 2014).

Fig. 2 shows lidar measurements carried out from 16:00 to 18:00 UTC on 19 June 2011. We show profiles of the particle backscatter coefficient, and the linear volume and particle depolarization ratio. We obtained meteorological parameters from a radiosonde launched at 18:00 UTC. The volcanic aerosol layer shows a separation into two sub-layers that stretched between 15 km and 17 km height asl (vertical thickness less than about 2 km). The peak value of the particle backscatter coefficient of the aerosol layer was 1.5 ± 0.3 Mm^{-1} sr^{-1} (532 nm) at 16.4 km height asl. The maximum value of the linear volume and particle depolarization ratios were 1.9% and 2.2% in that height, respectively. The mean value of the linear particle depolarization ratio of the aerosol layer was 1.58%. This value is higher than the depolarization ratio caused by molecular scattering, which contributed approximately 0.44% to the total signal.

3.2.2. Case study of 3 August 2011: forty-four days after the first measurement

We could not perform lidar measurements from 20 June to 3 August 2011 because of the arrival of the monsoon front at our observation site, which usually is connected to strong clouds decks and heavy rain on a nearly daily basis. We continued with our lidar observations after the end of the monsoon.

Fig. 3 shows results of lidar and radiosonde measurements carried out on 3 August 2011. A multi-peak layered structure existed. The height of the main peak (in terms of the backscatter coefficient) had shifted to a slightly lower altitude compared to the observation on 19 June 2011. However, the most significant change of the volcanic aerosol layer compared to the first measurements on 11 June 2011 happened to the geometrical thickness (see Fig. 2). The geometrical depth of the aerosol layer was 9.5 km according to the profiles of the particle backscatter coefficient at 532 nm; the bottom height of the aerosol layer was at 10 km and the top height of the aerosol layer was at 19.5 km height asl. That means, the volcanic aerosol layer that had a single-peak and a narrow vertical thickness at the start of the eruption had changed into a multi-peak structure with comparably wide vertical thickness structure after two months. The maximum value of the particle backscatter coefficient had decreased to 0.17 ± 0.03 Mm^{-1} sr^{-1} (532 nm) and 0.03 ± 0.01 Mm^{-1} sr^{-1} (1064 nm) at 17.5 km height asl.

The profile of the linear particle depolarization ratio profile is different from the vertical profile of the particle backscatter coefficient. The maximum value of the linear particle depolarization ratio is at 12 km height asl as 1.9%, and the value of the linear particle depolarization ratio decreases with increasing height. The maximum value of the linear particle depolarization ratio is T 17 km height asl.

3.2.3. Time series

Fig. 4 shows the time-height contour plot of the range-corrected backscatter signals (532 nm, logarithmic scale), and examples of the vertical profiles of the particle backscatter coefficient and the linear particle depolarization ratio measured from 19 June to 7 October 2011.

At the beginning of the measurement period, on 19 and 20 June 2011, the geometrical depth of the aerosol layer was narrow, i.e. it was between 1 and 2 km. The peak value of the particle backscatter coefficient and the linear particle depolarization ratio was comparable high, i.e. 0.45–2.0 Mm^{-1} sr^{-1} and 1.2–2.0% at 532 nm, respectively. In addition, the altitude at which we detected the maximum values of the particle backscatter coefficient and the linear particle depolarization ratio were very similar. We conclude that the aerosol layers, which consisted of spherical and non-spherical particles were in a well-mixed state shortly of the volcanic eruption.

However, after approximately two months, i.e. from 3 August 2011 to the end of our measurements, the vertical thickness of the volcanic aerosol layer had expanded to a geometrical thickness of 10 km. In addition, the linear particle depolarization ratios showed

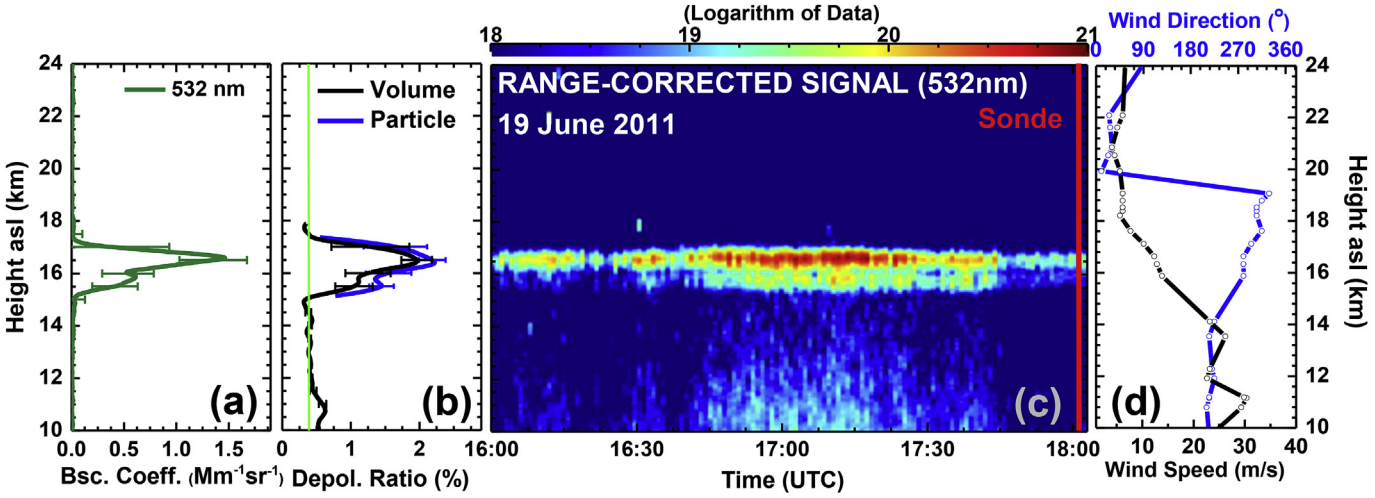

Fig. 2. The aerosol layer observed from 16:00 to 18:00 UTC on 19 June 2011. The two left panels show the particle backscatter coefficient at 532 nm (a) and the linear volume and particle depolarization ratio at 532 nm (b). Error bars denote the precision at each point (1 standard deviation). The green vertical line in (b) indicates the molecular depolarization ratio of 0.44% at 532 nm. The middle panel shows the aerosol layer in terms of the 532 nm range-corrected backscatter signal (in arbitrary units) as a function of height and time (c). The red line in (c) indicates the time of the radiosonde launch (at 18:00 UTC). The two right panels show the radiosonde profiles. Wind speed and wind direction are shown in (d). (For interpretation of the references to colour in this figure legend, the reader is referred to the web version of this article.)

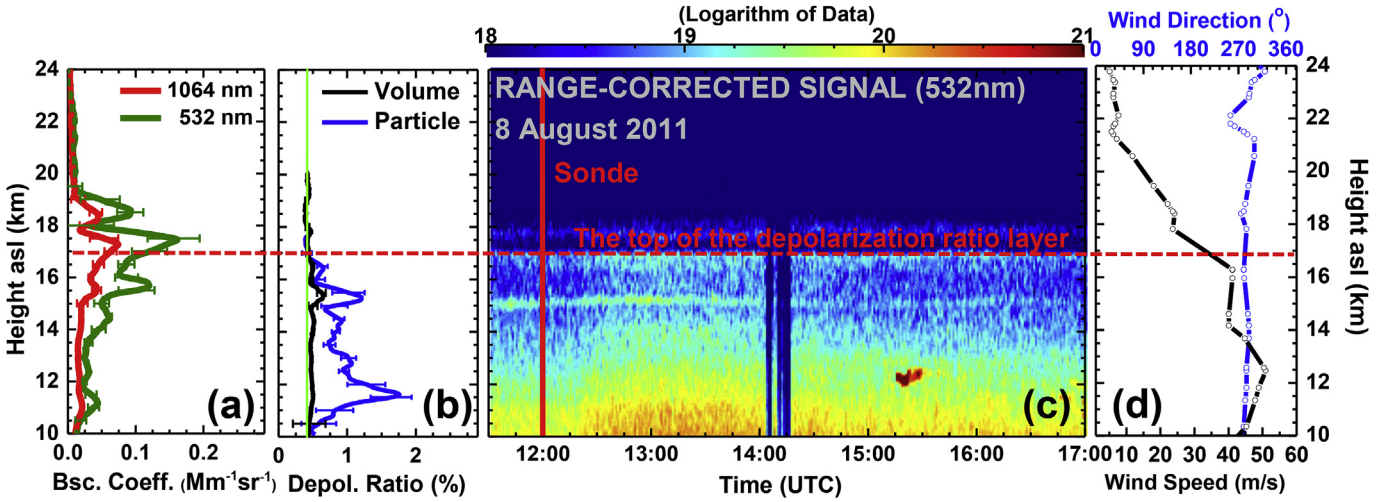

Fig. 3. Same as Fig. 2 except for the measurement period from 11:30 to 17:00 UTC on 3 August 2011. Meteorological parameters (c and d) were measured with a radiosonde launched at 12:00 UTC.

consistently higher values in the lower part of the aerosol layer compared to the values in the upper part of the aerosol layer (Sassen et al., 1989; Sassen and Horel, 1990). We conclude that the upper part of the volcanic aerosol layer mainly cotained spherical particles which are sulfuric acid droplets produced through photochemical reactions in the stratosphere. In contrast, the lower part of the volcanic aerosol layer contained a relatively high proportion of non-spherical particles compared to the number of non-spherical particles in the upper part of the layer.

One possible interpretation of this result can be as follows: different time-dependent dynamical processes act on the vertical dispersion of the volcanic aerosol layer in the UT and LS. In the early stages of the measurement period, shortly after the volcanic eruption, the vertically thin aerosol plumes were distributed by vertical eddy diffusion from mesoscale and small-scale turbulence (Bitar et al., 2010; Holton et al., 1995). As time passed by the aerosol layers became vertically thicker, however the aerosols were not dispersed uniformly throughout the volcanic aerosol layer. It seems as if non-spherical particles in the volcanic aerosol layer moved downward more easily than spherical particles as the result of gravitational sedimentation. Rather high wind speeds in the lower part of the aerosol layer may have accelerated this gravitational sedimentation (see Fig. 4 (e)). .

At this point, we doubt that pure ash particles from the Nabro eruption were injected into the UT and LS. The linear particle depolarization ratio of the volcanic aerosol layer is smaller than the 10–40% linear particle depolarization ratio of ash particles which consist of glass- and mineral particles (Groβ et al., 2012; Miffre et al., 2012). Although the volcanic aerosol particles do not consist of pure ash, the linear particle depolarization ratios in Fig. 4 (c) indicate that non-spherical particles were present in the volcanic plume.

We assume that this aerosol type of non-spherical particles is formed by the following processes, though our limited set of data does not allow for an unambiguous explanation. One potential cause may be the freezing of sulfuric acid particles (Reiter et al., 1979) and the other reason may be the crystallized particles in the form of ammonium sulfate particles ($(NH_4)_2SO_4$) which may have contributed in a small portion to the stratospheric aerosol particles during the pre-Nabro eruption (Iwasaka and Hayashida, 1981). Another, third reason may be inhomogeneous haze particles (Iwasaka, 1986).

3.3. AOD

Fig. 5 shows the temporal variation of the AOD (at 532 nm) of the volcanic aerosol layers and the maximum values of the particle backscatter coefficient of the volcanic aerosol layers in the UT and LS observed from June 2011 to December 2011.

Our first measurement (19 June 2011), i.e., 7 days after the Nabro eruption (see Fig. 2) shows the largest values; the AOD was 0.07 and the maximum particle backscatter coefficient was 1.5 ± 0.3 $Mm^{-1}sr^{-1}$. The following day, the maximum AOD and the maximum particle backscatter coefficient suddenly dropped to 0.01 and 0.4 ± 0.08 $Mm^{-1}sr^{-1}$, respectively. This sudden drop indicates that the initial distribution of the Nabro aerosol plume was horizontally inhomogeneous. Lidar observations at two Japanese sites (Tsukuba: 36.05° N, 140.13° E and Saga: 33.24° N, 130.29° E) and one site in China (Wuhan: 30.5° N, 114.4° E) also show that the vertical distribution and intensity of the volcanic plume varied strongly until August 2011 (Zhuang and Yi, 2016; Uchino et al., 2012).

In the early stage of our measurements, the high variability of the AOD may have been caused by the non-uniform distribution of the particles over East Asia (Zhuang and Yi, 2016). About two months later, the AOD and maximum particle backscatter coefficient gradually decreased with time. The volcanic aerosol layer displayed a single-peak structure. The geometrical width increased with time from September 2012 onward (See Fig. 4 (c)) which indicates the vertical dispersion of the Nabro volcanic aerosol particles.

Fig. 5 shows that the AOD decreased from August onward. A polynomial regression fit was carried out and we found an e-folding decay time of 117 days. This e-folding decay time agrees with the 130 days found for the time series of the integrated backscatter coefficient observed at Wuhan, China (Zhuang and Yi, 2016). This decay time considerably shorter than the e-folding time reported for stratospheric aerosol plume caused by the Mt. Pinatubo eruption. Studies of the Pinatubo volcano aerosol layer showed an e-folding time of approximately 1 year (Ansmann et al., 1997; Uchino et al., 1995) which is much longer than the e-folding time of the Nabro volcano aerosol layer. Zhuang and Yi (2016) explain this difference on the basis of the different injection heights of the plumes ejected by Mt. Nabro and Mt. Pinatubo. The Mt. Nabro aerosol layers observed at our lidar site and at many

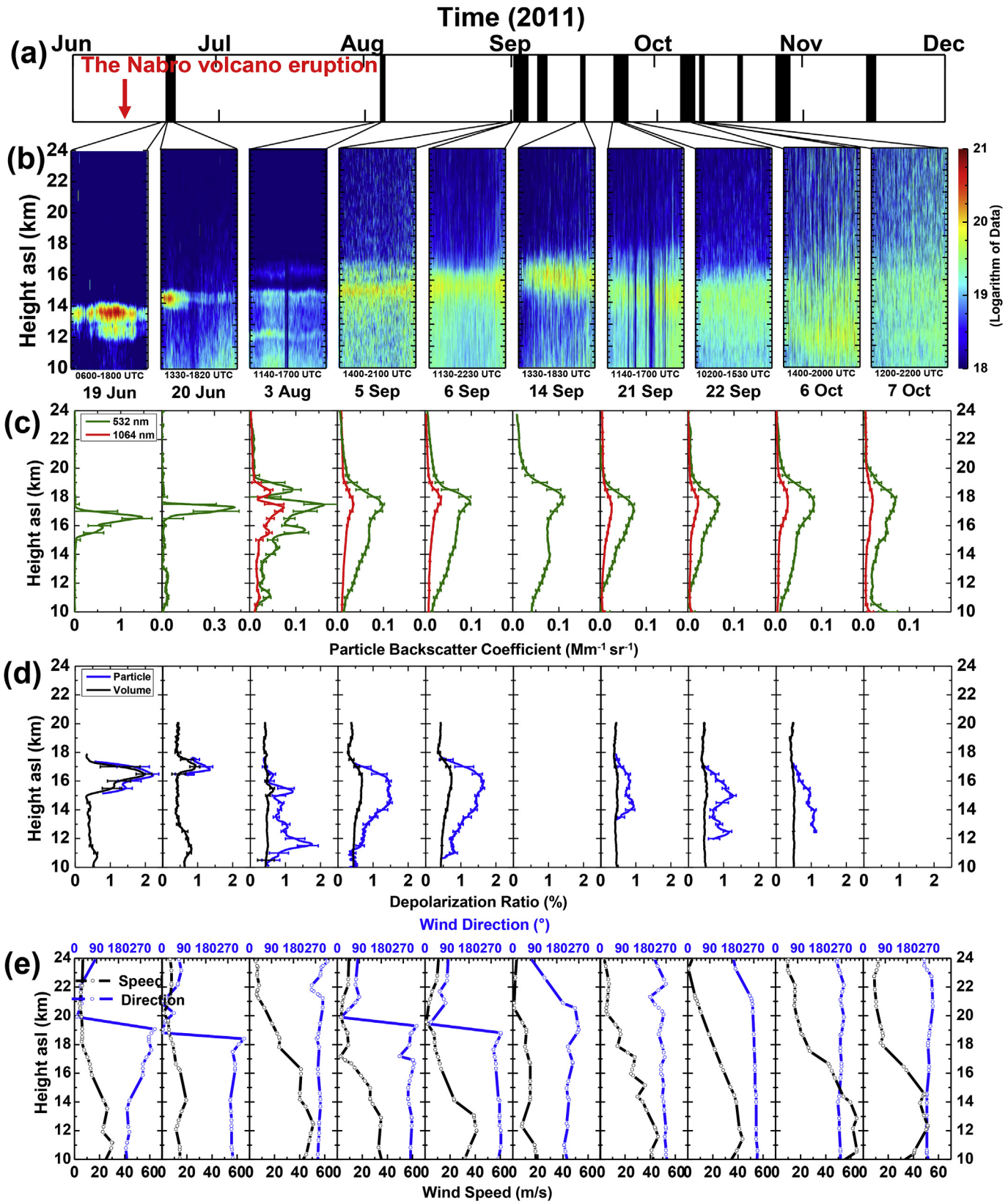

Fig. 4. (a) Time series of measurements taken between 19 June and 7 October 2011. (b) Contour plot (time-height) of the range-corrected backscatter signal at 532 nm. (c) Profiles of the particle backscatter coefficient at 532 nm and 1064 nm. (d) Profiles of the linear particle depolarization ratio and the total depolarization ratio (particles plus molecules) at 532 nm. Because of low signal-to-noise ratios of the cross-polarized signals at 532 nm, profiles of the linear particle depolarization ratio are not shown for the measurements carried out on 14 September and 7 October. (e) Wind speed and wind direction.

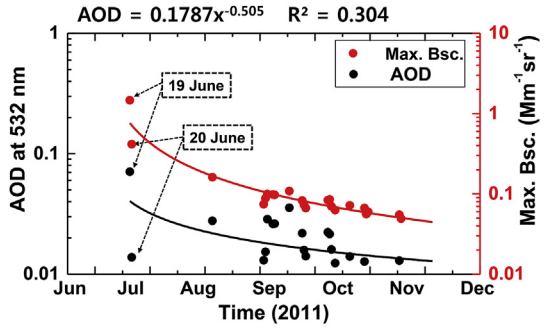

Fig. 5. Temporal variation of the aerosol optical depth (AOD) at 532 nm (closed black circles) and the maximum backscatter coefficient at 532 nm (closed red circles) of the aerosol layers in the UT and LS. (For interpretation of the references to colour in this figure legend, the reader is referred to the web version of this article.)

other locations resided in an altitude range between 15 and 20 km (Sawamura et al., 2012; Uchino et al., 2012; Zhuang and Yi, 2016). This result suggests that the Nabro aerosol plumes initially had formed at altitudes below 20 km where stratosphere-troposphere exchange (STE) processes and gravitational settling jointly caused a fast removal of the aerosols.

In contrast, the Mt. Pinatubo aerosol plumes had initially been generated in an altitude range between 20 and 30 km (Ansmann et al., 1997) where only gravitational sedimentation acted and relatively slowly removed the aerosol particles in that height range (Zhuang and Yi, 2016). Vertical wind speed variations, as shown in Fig. 4(e) support our finding. The wind speed decreases with increasing altitude. High wind speeds in the LT can contribute to particle diffusion.

4. Summary and conclusions

This research work presents results of lidar measurements of the variation of the geometrical height and width of an volcanic aerosol layer and its evolution with time in the UT and LS. The aerosol layer was injected into the stratosphere by the eruption of the Nabro volcano (Eritrea, East Africa). The volcanic plume was observed at our site in Gwangju, Korea, for the first time on 19 June 2011, seven days after the first eruption on 12 June 2011. The variation of the vertical structure of the stratospheric aerosol layer was analysed on the basis of the particle backscatter coefficients and the linear particle depolarization ratio.

We find that the variation of the particle backscatter coefficient and the linear particle depolarization ratio of the volcanic aerosol layers occurred in the UT and LS in two stages (with respect to their temporal variation). On 19 and 20 June 2011, which can be defined as the period during which the stratospheric aerosol layer expanded over Gwangju, the volcanic plume formed a geometrically thin layer of approximately 2-km thickness between 15 km and 17 km height asl. The peak value of the particle backscatter coefficient of the aerosol layer was 1.5 ± 0.3 Mm^{-1} sr^{-1} (532 nm) at 16.4 km height asl. We found the maximum value of the linear volume and the particle depolarization ratios in the same height. Values were 1.9% and 2.2% in that height, respectively. The value of the linear particle depolarization ratio indicates that non-spherical particles were present in the volcanic plume. However, these particles were not pure ash particles.

The AOD varied strongly in early stage of our measurement period. This variation shows that the volcanic plume was not uniformly distributed over East Asia. However, about two months after we started our observations the vertical profile of the volcanic aerosol layer had changed significantly. The maximum value of the particle backscatter coefficient had decreased and the (vertical) geometrical depth of the volcanic aerosol layer had increased compared to the situation at the beginning of our observations (expansion period). The volcanic aerosol layer reached between 10 and 19.5 km height, i.e. its geometrical thickness was 9.5 km, whereas its geometrical thickness was 1–2 km at the beginning of the lidar observations. The linear particle depolarization ratios was higher in the lower part of the aerosol layer compared to the values in the upper part. The maximum value of the backscatter coefficient was found in the upper part of the volcanic aerosol layer. Non-spherical particles were continuously present in the lower part of the volcanic aerosol layer until the end of our measurement period. The vertical distribution of the linear particle depolarization ratio indicates that gravitational sedimentation may have led to a faster downward movement of the non-spherical particles in the volcanic aerosol layer compared to the spherical particles. Rather high wind speeds in the lower part of the aerosol layer may have accelerated this gravitational sedimentation. High wind speeds lead to greater wind shear and therefore stronger turbulence, which may lead to stronger downward draft of these non-spherical particles (stronger frictional forces compared to spherical particles). Wind speed in that sense might not affect gravitational settling which is not a direct effect of wind speed but an effect of the gravitational field of Earth.

The AOD decreased gradually with time until the end of our measurement period. We find an e-folding decay time of 117 days on the basis of a polynomial regression fit of AOD. We assume that the injection of the particles into the stratosphere happened in a way in which spherical and non-spherical particles were well mixed. The geometrical depth of the volcanic plume was low. As time went by, the volcanic aerosol layer expanded downward as the result of gravitational sedimentation. At this point of time, the non-spherical particles seemed to have responded to gravitational sedimentation stronger than their spherical counterparts, if we consider the vertical distribution of the linear particle depolarization ratio. Our study adds to the limited information about optical properties and spatial characteristic of volcanic aerosols over East Asia. Our results may also become important reference data for future measurements of volcanic eruptions in East Asia, i.e. in source regions which are part of the West Pacific Rim (Ring of Fire) where a large number of volcanic eruptions frequently occurs.

Acknowledgements

This work was funded by the Korea Meteorological Administration Research and Development Program under Grant KMIPA2015-6150. This work was supported by a National Research Foundation of Korea grant funded by the Korean government (MEST) (NRF-2015R1D1A1A09058269). This research was also supported by the International Environmental Research Center (IERC). We thank the Department of Atmospheric Science at the University of Wyoming for providing the radiosonde data (http://weather.uwyo.edu/upperair/sounding.html).

References

Ansmann, A., Mattis, I., Wandinger, U., Wagner, F., Reichardt, J., Deshler, T., 1997. Evolution of the Pinatubo aerosol: Raman lidar observations of particle optical depth, effective radius, mass, and surface area over Central Europe at 53.4 N. J. Atmos. Sci. 54, 2630–2641.

Ansmann, A., Tesche, M., Groß, S., Freudenthaler, V., Seifert, P., Hiebsch, A., Schmidt, J., Wandinger, U., Mattis, I., Müller, D., 2010. The 16 April 2010 major volcanic ash plume over central Europe: EARLINET lidar and AERONET photometer observations at Leipzig and Munich, Germany. Geophys. Res. Lett. 37.

Barnes, J., Hofmann, D., 2001. Variability in the stratospheric background aerosol over Mauna Loa observatory. Geophys. Res. Lett. 28, 2895–2898.

Behrendt, A., Nakamura, T., 2002. Calculation of the calibration constant of polarization lidar and its dependency on atmospheric temperature. Opt. express 10, 805–817.
Biele, J., Beyerle, G., Baumgarten, G., 2000. Polarization lidar: correction of instrumental effects. Opt. express 7, 427–435.
Bitar, L., Duck, T., Kristiansen, N., Stohl, A., Beauchamp, S., 2010. Lidar observations of Kasatochi volcano aerosols in the troposphere and stratosphere. J. Geophys. Res. Atmos. 115.
Bluth, G.J., Doiron, S.D., Schnetzler, C.C., Krueger, A.J., Walter, L.S., 1992. Global tracking of the SO2 clouds from the June, 1991 mount Pinatubo eruptions. Geophys. Res. Lett. 19, 151–154.
Clarisse, L., Hurtmans, D., Clerbaux, C., Hadji-Lazaro, J., Ngadi, Y., Coheur, P.-F., 2012. Retrieval of sulphur dioxide from the infrared atmospheric sounding interferometer (IASI). Atmos. Meas. Tech. 5, 581–594.
Draxler, R.R., Hess, G., 1997. Description of the HYSPLIT4 Modeling System.
Draxler, R.R., Hess, G., 1998. An overview of the HYSPLIT_4 modelling system for trajectories. Aust. Meteorol. Mag. 47, 295–308.
Fairlie, T., Vernier, J.-P., Natarajan, M., Bedka, K., 2014. Dispersion of the Nabro volcanic plume and its relation to the Asian summer monsoon. Atmos. Chem. Phys. 14, 7045–7057.
Fernald, F.G., 1984. Analysis of atmospheric lidar observations: some comments. Appl. Opt. 23, 652–653.
Freudenthaler, V., Esselborn, M., Wiegner, M., Heese, B., Tesche, M., Ansmann, A., Müller, D., Althausen, D., Wirth, M., Fix, A., 2009. Depolarization ratio profiling at several wavelengths in pure Saharan dust during SAMUM 2006. Tellus B 61, 165–179.
Groß, S., Freudenthaler, V., Wiegner, M., Gasteiger, J., Geiß, A., Schnell, F., 2012. Dual-wavelength linear depolarization ratio of volcanic aerosols: Lidar measurements of the Eyjafjallajökull plume over Maisach, Germany. Atmos. Environ. 48, 85–96.
Guo, S., Bluth, G.J., Rose, W.I., Watson, I.M., Prata, A., 2004. Re-evaluation of SO2 release of the 15 June 1991 Pinatubo eruption using ultraviolet and infrared satellite sensors. Geochem. Geophys. Geosystems 5.
Hofmann, D.J., Solomon, S., 1989. Ozone destruction through heterogeneous chemistry following the eruption of El Chichon. J. Geophys. Res. Atmos. 94, 5029–5041.
Hofmann, D., Barnes, J., O'Neill, M., Trudeau, M., Neely, R., 2009. Increase in background stratospheric aerosol observed with lidar at Mauna Loa Observatory and Boulder, Colorado. Geophys. Res. Lett. 36.
Holton, J.R., Haynes, P.H., McIntyre, M.E., Douglass, A.R., Rood, R.B., Pfister, L., 1995. Stratosphere-troposphere exchange. Rev. Geophys. 33, 403–439.
Iwasaka, Y., 1986. Measurement of depolarization of stratospheric particles by lidar-A case study on the disturbed stratospheric aerosol layer by the volcanic eruption of Mt. El Chichon. J. geomagnetism Geoelectr. 38, 729–740.
Iwasaka, Y., Hayashida, S., 1981. The effects of the volcanic eruption of St. Helens on the polarization properties of stratospheric aerosols-Lidar measurement at Nagoya. Meteorological Soc. Jpn. J. 59, 611–614.
Klett, J.D., 1985. Lidar inversion with variable backscatter/extinction ratios. Appl. Opt. 24, 1638–1643.
Mattis, I., Tesche, M., Grein, M., Freudenthaler, V., Müller, D., 2009. Systematic error of lidar profiles caused by a polarization-dependent receiver transmission: quantification and error correction scheme. Appl. Opt. 48, 2742–2751.
Mattis, I., Siefert, P., Müller, D., Tesche, M., Hiebsch, A., Kanitz, T., Schmidt, J., Finger, F., Wandinger, U., Ansmann, A., 2010. Volcanic aerosol layers observed with multiwavelength Raman lidar over central Europe in 2008–2009. J. Geophys. Res. Atmos. 115.
McCormick, M.P., Thomason, L.W., Trepte, C.R., 1995. Atmospheric effects of the Mt Pinatubo eruption. Nature 373, 399–404.
Miffre, A., David, G., Thomas, B., Rairoux, P., Fjaeraa, A., Kristiansen, N., Stohl, A., 2012. Volcanic aerosol optical properties and phase partitioning behavior after long-range advection characterized by UV-Lidar measurements. Atmos. Environ. 48, 76–84.
Müller, D., Mattis, I., Tatarov, B., Noh, Y., Shin, D., Shin, S., Lee, K., Kim, Y., Sugimoto, N., 2010. Mineral quartz concentration measurements of mixed mineral dust/urban haze pollution plumes over Korea with multiwavelength aerosol Raman-quartz lidar. Geophys. Res. Lett. 37.
Noh, Y.M., 2014. Single-scattering albedo profiling of mixed Asian dust plumes with multiwavelength Raman lidar. Atmos. Environ. 95, 305–317.
Noh, Y.M., Kim, Y.J., Müller, D., 2008. Seasonal characteristics of lidar ratios measured with a Raman lidar at Gwangju, Korea in spring and autumn. Atmos. Environ. 42, 2208–2224.
Noh, Y.M., Müller, D., Mattis, I., Lee, H., Kim, Y.J., 2011. Vertically resolved light-absorption characteristics and the influence of relative humidity on particle properties: multiwavelength Raman lidar observations of East Asian aerosol types over Korea. J. Geophys. Res. 116, D06206. http://dx.doi.org/10.1029/2010JD014873.
Parker, D., Wilson, H., Jones, P.D., Christy, J., Folland, C.K., 1996. The impact of Mount Pinatubo on world-wide temperatures. Int. J. Climatol. 16, 487–497.
Polissar, A.V., Hopke, P.K., Harris, J.M., 2001. Source regions for atmospheric aerosol measured at Barrow, Alaska. Environ. Sci. Technol. 35, 4214–4226.
Reiter, R., Jäger, H., Carnuth, W., Funk, W., 1979. The stratospheric aerosol layer observed by lidar since October 1976. A contribution to the problem of hemispheric climate. Arch. für Meteorol. Geophys. Bioklimatol. Ser. B 27, 121–149.
Robock, A., 2000. Volcanic eruptions and climate. Rev. Geophys. 38, 191–219.
Rodriguez, J.M., Ko, M.K., Sze, N.D., 1991. Role of Heterogeneous Conversion of N2O5 on Sulphate Aerosols in Global Ozone Losses.
Sassen, K., Horel, J.D., 1990. Polarization lidar and synoptic analyses of an unusual volcanic aerosol cloud. J. Atmos. Sci. 47, 2881–2889.
Sassen, K., Zhao, H., Yu, B.-K., 1989. Backscatter laser depolarization studies of simulated stratospheric aerosols: crystallized sulfuric acid droplets. Appl. Opt. 28, 3024–3029.
Sawamura, P., Vernier, J.-P., Barnes, J., Berkoff, T., Welton, E., Alados-Arboledas, L., Navas-Guzmán, F., Pappalardo, G., Mona, L., Madonna, F., 2012. Stratospheric AOD after the 2011 eruption of Nabro volcano measured by lidars over the Northern Hemisphere. Environ. Res. Lett. 7, 034013.
Shin, D., Noh, Y., Tatarov, B., Shin, S., Kim, Y., Müller, D., 2010. Multiwavelength aerosol raman lidar for optical and microphysical aerosol typing over east asia. Proc. Int. Laser Radar Conf. 239–242.
Shin, S., Müller, D., Lee, C., Lee, K., Shin, D., Kim, Y., Noh, Y., 2015. Vertical variation of optical properties of mixed Asian dust/pollution plumes according to pathway of air mass transport over East Asia. Atmos. Chem. Phys. 15, 6707–6720.
Smithsonian Institution. Global Volcanism Program. http://volcano.si.edu/world/volcano.cfm%3fvnum%3d0201%5f101%26volpage%3dvar.
Solomon, S., Sanders, R., Garcia, R., Keys, J., 1993. Increased Chlorine Dioxide over Antarctica Caused by Volcanic Aerosols from Mount Pinatubo.
Stein, A., Draxler, R., Rolph, G., Stunder, B., Cohen, M., Ngan, F., 2015. NOAA's HYSPLIT atmospheric transport and dispersion modeling system. Bull. Am. Meteorological Soc. 96, 2059–2077.
Tatarov, B., Müller, D., Shin, D.H., Shin, S.K., Mattis, I., Seifert, P., Noh, Y.M., Kim, Y., Sugimoto, N., 2011. Lidar measurements of Raman scattering at ultraviolet wavelength from mineral dust over East Asia. Opt. express 19, 1569–1581.
Tesche, M., Gross, S., Ansmann, A., Mueller, D., Althausen, D., Freudenthaler, V., Esselborn, M., 2011. Profiling of Saharan dust and biomass-burning smoke with multiwavelength polarization Raman lidar at Cape Verde. Tellus B 63, 649–676.
Uchino, O., Nagai, T., Fujimoto, T., Matthews, W., Orange, J., 1995. Extensive lidar observations of the Pinatubo aerosol layers at Tsukuba (36.1 N), Naha (26.2 N), Japan and Lauder (45.0 S), New Zealand. Geophys. Res. Lett. 22, 57–60.
Uchino, O., Sakai, T., Nagai, T., Nakamae, K., Morino, I., Arai, K., Okumura, H., Takubo, S., Kawasaki, T., Mano, Y., 2012. On recent (2008–2012) stratospheric aerosols observed by lidar over Japan. Atmos. Chem. Phys. 12, 11975–11984.
Wandinger, U., Ansmann, A., Reichardt, J., Deshler, T., 1995. Determination of stratospheric aerosol microphysical properties from independent extinction and backscattering measurements with a Raman lidar. Appl. Opt. 34, 8315–8329.
Wu, P.-M., Okada, K., Tanaka, T., Sasaki, T., Nagai, T., Fujimoto, T., Uchino, O., 1994. Balloon observation of stratospheric aerosols over Tsukuba, Japan Two years after the Pinatubo volcanic eruption. J. Meteor. Soc. Jpn. 72, 475–480.
Zhuang, J., Yi, F., 2016. Nabro aerosol evolution observed jointly by lidars at a mid-latitude site and CALIPSO. Atmos. Environ. 140, 106–116.